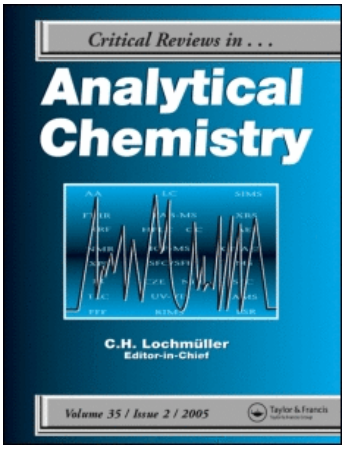

Critical Reviews in Analytical Chemistry
Publication details, including instructions for authors and subscription information:
http://www.informaworld.com/smpp/title~content=t713400837

Advances in Multifrequency Phase and Modulation Fluorescence Analysis

Frank V. Bright[a]; Thomas A. Betts[a]; Kevin S. Litwiler[a]
[a] Department of Chemistry at SUNY-Buffalo, Buffalo, NY

To cite this Article Bright, Frank V. , Betts, Thomas A. and Litwiler, Kevin S.(1990) 'Advances in Multifrequency Phase and Modulation Fluorescence Analysis', Critical Reviews in Analytical Chemistry, 21: 6, 389 — 405
To link to this Article: DOI: 10.1080/10408349008051635
URL: http://dx.doi.org/10.1080/10408349008051635

Advances in Multifrequency Phase and Modulation Fluorescence Analysis

Frank V. Bright, Thomas A. Betts, and Kevin S. Litwiler

I. INTRODUCTION

The first report of luminescence is credited to the Spanish physician, Monardes, who in 1565 noted that water contained in a wooden cup made from *Ligirium nephiticiem* exhibited a strange blue shimmer. Today, 325 years later, scientists are still using the emissive characteristics (spectral, temporal, and polarization) of fluorophores to probe directly and indirectly many diverse physical phenomena. Over the years, the utility of fluorescence measurements has made a tremendous impact in numerous subdisciplines of chemistry. For further information into this diverse area, the interested reader is encouraged to consult the many reviews and textbooks in the field.[1-8]

In this review, we focus on the analytical aspects of frequency-domain fluorescence spectroscopy. To this end, we divide our discussion into the following sections:

1. The recovery of fluorescence decay times and rotational diffusion information from frequency-domain data
2. Advances in multifrequency phase and modulation instrumentation
3. Selected applications of frequency-domain fluorescence spectroscopy to chemical analysis
4. A prospectus for future advances and applications

II. THEORY

Under standard conditions, virtually all species occupy the ground electronic state. When photon energy is coincident with the energy of an allowed electronic transition, a small fraction of the ground-state population is promoted to excited electronic states. The excited states subsequently de-excite back to the ground state over numerous pathways. Many of these are nonradiative; however, there are two emissive paths back to the ground state, fluorescence and phosphorescence. Phosphorescence is the emission from an excited triplet state to the ground state, which is a singlet state. Because this is a forbidden transition, the emissive rate is slow, thus the decay times are relatively long (milliseconds to seconds). Unlike phosphorescence, fluorescence is an allowed singlet-to-singlet transition and occurs rapidly (nanoseconds). In this review, our focus is fluorescence; however, all of the same approaches have been used for phosphorescence as well.

Fluorescence is characterized by several parameters, most notably:

1. The excitation wavelength (λ_{ex})
2. The emission wavelength (λ_{em})
3. The steady-state polarization (P) or anisotropy (r)
4. The lifetime (τ)
5. The rotational correlation time (ϕ)

Of these, the latter two reflect the time-course of the emission process. In condensed phase systems, these two processes typically occur in 10^{-8} to 10^{-13} s. As a result, any process which occurs on a similar time scale (as fluorescence) can perturb the fluorescence process. For example, processes like collisional quenching, energy transfer, solvent relaxation, and rotational diffusion all occur on the fluorescence time scale. Thus, an excited-state fluorophore can be used to report on its local environment and how that environment changes with time. This information then provides insight into important processes occurring on the nanosecond and sub-nanosecond time scale.

A. Discrete Lifetimes

Assume that a given sample contains n noninteracting fluorescent species (components). Following excitation with an optically short Dirac delta function, we can describe the time-dependent emission intensity (I(t)) by a multiple exponential decay of the form:[9]

$$I(t) = \sum_{i=1}^{n} a_i \exp(-t/\tau_i) \quad (1)$$

where a_i is a pre-exponential factor that represents the fractional contribution of component, i, with lifetime τ_i, to the total time-resolved decay. The fractional contribution to the total intensity (f_i) of each species is

$$f_i = a_i\tau_i \Big/ \sum_{i=1}^{n} a_i\tau_i. \quad (2)$$

Frank V. Bright received his B.S. degree from the University of Redlands, his Ph.D. from Oklahoma State University, and was a Postdoctoral Fellow at Indiana University. Dr. Bright is an Assistant Professor in the Department of Chemistry at SUNY-Buffalo, Buffalo, NY. **Thomas A. Betts** received his B.S. from Clarion University and is presently a Graduate Research Associate in the Department of Chemistry at SUNY-Buffalo, Buffalo, NY. **Kevin S. Litwiler** received his B.S. from Clarion University and is presently a Graduate Research Associate in the Department of Chemistry at SUNY-Buffalo, Buffalo, NY.

Of course, nonexponential decays are observed in what are often assumed to be simple systems because of competing processes (e.g., solvent relaxation). In this review we restrict our initial discussion to the simpler exponential or multiexponential decay processes (Equation 1).

In the frequency domain, the sample under study is excited with sinusoidally, amplitude-modulated light.[10-12] Typically, these frequencies span the mega- to gigahertz regions and have been generated using many devices (Table 1). The resulting fluorescence emission (Em(t)) is equal in frequency to the excitation waveform (Ex(t)), but is phase shifted (Θ) and amplitude demodulated (M) to an extent dependent on the fluorescence lifetime(s) of the sample (Figure 1). A simple analogy can be drawn here between the response of a fluorescent sample and the response of a simple resistance-capacitance (RC) circuit to a high frequency (noise) signal. In an RC circuit, a high-frequency modulated input is phase shifted and demodulated to an extent dependent on the circuit RC time constant.[13] With respect to fluorescence, the time constant is analogous to the fluorescence lifetime(s) of the sample.

Table 1
Methods Used to Generate Sinusoidally Modulated Light

Device	Comments
Kerr cell	First device used to modulate light at high frequency. The device is unsuitable for UV work and is temperature sensitive. The frequency bandwidth is broad.
Debye-Sears acousto-optic	A large aperture device with fast optics. Operates on resonance frequencies. Upper frequency limited to about 50 MHz.
Piezo-optical	A large aperture device with slightly slower optics than a Debye-Sears. Can be set up to give ω or 2ω.
Electro-optic (Pockel's cell)	A small aperture device that is well suited for lasers or well collimated arc lamp excitation. Modulation to 250 MHz is possible.
CW laser	The sinusoidal modulations are produced at cavity resonant frequenices given by f(n) = nc/2L where n is an integrer, L is the cavity length, and c is the speed of light. The depth of modulation is poor, but continues up to the bandwidth of the lasing medium.
Mode-locked laser	The harmonic content of the mode-locked pulse train is used as the sinusoidally modulated source. The frequency conditions are the same as the CW case. In conjunction with synchronous pumping and cavity dumping, one can achieve intra-frequency separations of a few MHz and bandwidths near 100 GHz.
Synchrotron	The harmonic content of the synchrotron pulse is used as in the previous two cases; the spectral output is excellent and covers the UV and visible efficiently; the cost is prohibitive and the upper frequency limit is about 500 MHz

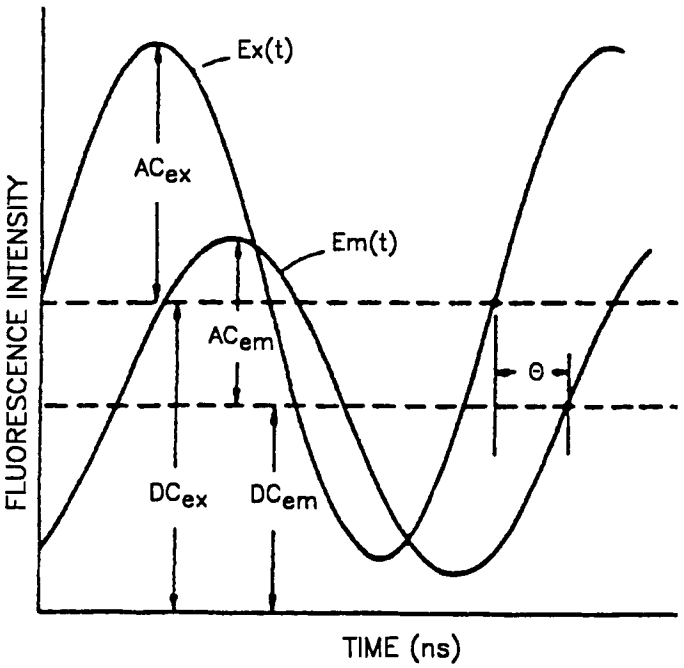

FIGURE 1. Schematic of the excitation (Ex(t)) and emission (Em(t)) of a fluorescent sample excited with sinusoidally modulated light. The phase shift and demodulation factor are given by Θ and $[(AC_{em}/DC_{em})/(AC_{ex}/DC_{ex})]$, respectively.

For any decay process the calculated (subscript c) values of Θ and M are given by[14]

$$\Theta_c(\omega) = \arctan (S(\omega)/C(\omega)) \quad (3)$$

$$M_c(\omega) = (S(\omega)^2 + C(\omega)^2)^{1/2} \quad (4)$$

where, for a single exponential decay:

$$S(\omega)/C(\omega) = \omega\tau \quad (5)$$

and

$$S(\omega)^2 + C(\omega)^2 = (1 + \omega^2\tau^2)^{-1} \quad (6)$$

For the general decay model shown by Equation 1, the frequency-dependent sine (S(ω)) and cosine (C(ω)) Fourier transforms are given by[14]

$$S(\omega) = \int_0^\infty I(t)\sin \omega t \, dt \quad (7)$$

$$C(\omega) = \int_0^\infty I(t)\cos \omega t \, dt \quad (8)$$

The decay times are recovered by experimentally measuring $\Theta_m(\omega)$ and $M_m(\omega)$ values while interrogating the sample at

several different angular modulation frequencies (ω; = $2\pi f$, f is the linear modulation frequency in Hz), followed by analysis using nonlinear least squares techniques.[15-17] In this approach, the sum of the squared difference between the calculated ($\Theta_c(\omega)$ and $M_c(\omega)$) and measured ($\Theta_m(\omega)$ and $M_m(\omega)$) values are minimized using the chi-squared (χ^2) function:

$$\chi^2 = \frac{1}{D}\sum_{\omega}\left(\frac{\Theta_m(\omega) - \Theta_c(\omega)}{v_\Theta^2}\right)^2 + \frac{1}{D}\sum_{\omega}\left(\frac{M_m(\omega) - M_c(\omega)}{v_m^2}\right)^2 \quad (9)$$

Here v_Θ and v_M are the variances in phase angle and demodulation, respectively, and D is the number of degrees of freedom. When v_Θ and v_M reflect accurately the uncertainty in the Θ and M experimental measurements, the goodness of fit is judged by the closeness of χ^2 to unity and random distribution of the residual phase angle and demodulation factor about zero.

Figure 2 shows a typical multifrequency phase and modulation data set collected in our laboratory for a synthetic binary mixture of POPOP and anthracene in ethanol. Panel A shows the experimental multifrequency phase angle and demodulation data (solid points) and the best fits to single (dotted line) and double exponential (solid line) decay models. Clearly, the single exponential fit is poor (χ^2 = 116) and is readily dismissed as an accurate representation of the sample decay kinetics. In contrast, the double exponential fit is quite good (χ^2 = 1.21). Further reduction in χ^2 is not realized by increasing the complexity of the model. Panels B and C in Figure 2 show the residual errors in phase angle and demodulation factor for these two fits, respectively. Again, it is evident from the systematic deviation of the residuals that the single exponential decay (dotted line) does not describe the experimental data. The double exponential model (solid line) fits the experimental data and results in randomly distributed residual error values. The recovered lifetimes for this particular mixture are 1.29 and 4.03 ns, which agree very well with the lifetimes for pure POPOP (1.35 ns) and anthracene (4.00 ns).

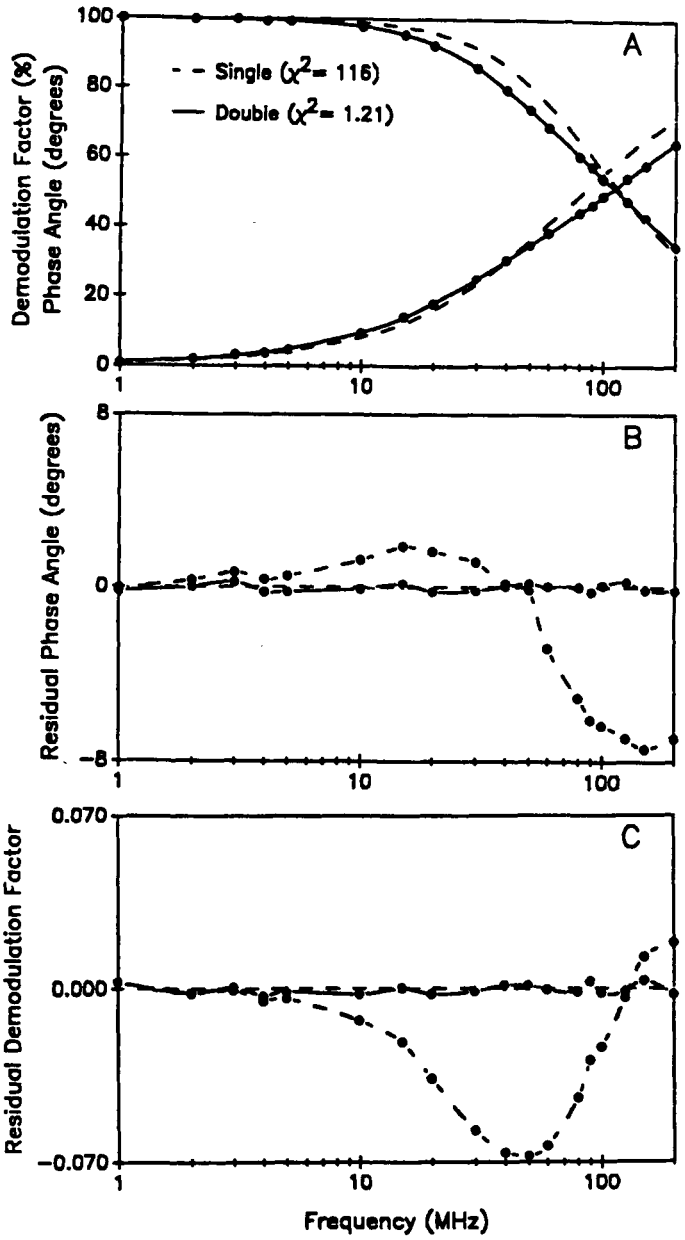

FIGURE 2. Typical multifrequency phase and modulation data for a binary mixture of POPOP and anthracene (A). Frequency-dependent residual errors in phase angle (B) and demodulation (C). Recovered lifetimes are 1.29 ns (47%) and 4.03 ns (53%).

B. Distributed Lifetimes

In the previous section, we considered the case of a few discrete emitting species that did not interconvert. Recently, the Ware,[18-20] Gratton,[21,22] and Lakowicz[23] groups have championed the idea of distributions of fluorescence lifetimes. In this approach, one goes beyond the simplistic view (Equation 1) of a fluorophore in a few discrete domains to the case where single or multiple fluorophores are located simultaneously in an ensemble of different microenvironments. The idea here is that the lifetime for many fluorophores varies significantly depending on the local environment. Thus, if a fluorophore were simultaneously located in an array or ensemble of environments, one would expect a distribution of lifetimes that paralleled the actual environmental distribution.

For a system consisting of n independent fluorescent centers the time-course of the fluorescence decay (I(t) is given by Equation 1, which can be rewritten by substitution of Equation 2 as

$$I(t) = \sum_{i=1}^{n} f_i \tau_i^{-1} \exp(-t/\tau_i) \quad (10)$$

For the case when the number of emitting centers is large, Equation 10 can be expressed as an integral of the form:

$$I(t) = \int_{\tau=0}^{\infty} f(\tau)\tau^{-1} \exp(-t/\tau)d\tau \quad (11)$$

Most approaches to the study of lifetime distributions assume that $f(\tau)$ is given by one of several distribution functions:

$$\text{Uniform:} \quad f(\tau) = A \quad \text{from } \tau' - W/2 \text{ to } \tau' + W/2 \quad (12)$$
$$f(\tau) = 0 \quad \text{at all other values}$$

or

$$\text{Gaussian:} \quad f(\tau) = A\{\exp[-(\tau - \tau')^2/2\sigma^2]/\sigma\sqrt{2\pi}\} \quad (13)$$

or

$$\text{Lorentzian:} \quad f(\tau) = A/\{1 + [(\tau - \tau')/(W/2)]^2\} \quad (14)$$

where τ' is the central or mean lifetime value, σ is the standard deviation of the Gaussian distribution, W is the full-width at half maximum (FWHM) for the Lorentzian and uniform distributions, τ is the lifetime, and A is an amplitude constant determined from the normalization condition:

$$f(\tau)d\tau = 1 \quad (15)$$

Figure 3 illustrates uniform, Gaussian, and Lorentzian lifetime distributions for a hypothetical system with a 5.0 ns central lifetime with standard deviation and FWHM of 1.5 ns. Further discussion of lifetime distribution analysis will be deferred until the Applications section.

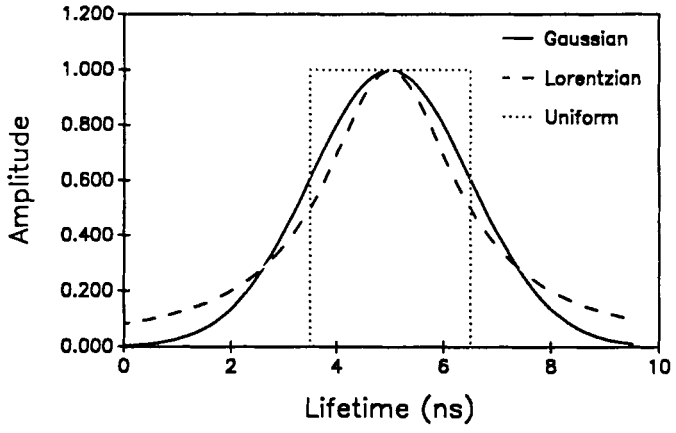

FIGURE 3. Uniform, Lorentzian, and Gaussian lifetime distributions for a hypothetical system with a mean lifetime of 5.0 ns and halfwidths or SD of 1.5 ns.

C. Rotational Diffusion

In the frequency domain, rotational diffusion information is recovered from the measured differential phase angle (Δ) and the polarized modulation amplitude ratio (Λ):[14,24]

$$\Delta(\omega) = \Theta_{\perp}(\omega) - \Theta_{\parallel}(\omega) \quad (16)$$

$$\Lambda(\omega) = m_{\parallel}(\omega)/m\perp(\omega) \quad (17)$$

where $\Theta_{\perp}$ and $\Theta_{\parallel}$ are the phase angles for the perpendicular and parallel components of the fluorescence and $m_{\parallel}$ and $m_{\perp}$ are the parallel and perpendicular components of the polarized modulation amplitudes, respectively.

In these experiments, vertically polarized, sinusoidally modulated light is used to excite the sample.[14,24] By analogy to the lifetime measurements, the polarized components of the fluorescence emission are phase shifted and amplitude demodulated, as shown in Figure 1. However, these components are each phase shifted and demodulated to different extents that depend on the rotational diffusion kinetics of the particular solute molecule.[14,24] This effect is illustrated in Figure 4.

For any intensity decay, I(t), it can be shown[25-27] that the time-resolved contribution of the parallel ($\parallel$) and perpendicular ($\perp$) components of the polarized emission are[25-27]

$$I_{\parallel}(t) = (1/3)I(t)(1 + 2r(t)) \quad (18)$$

$$I_{\perp}(t) = (1/3)I(t)(1 - r(t)) \quad (19)$$

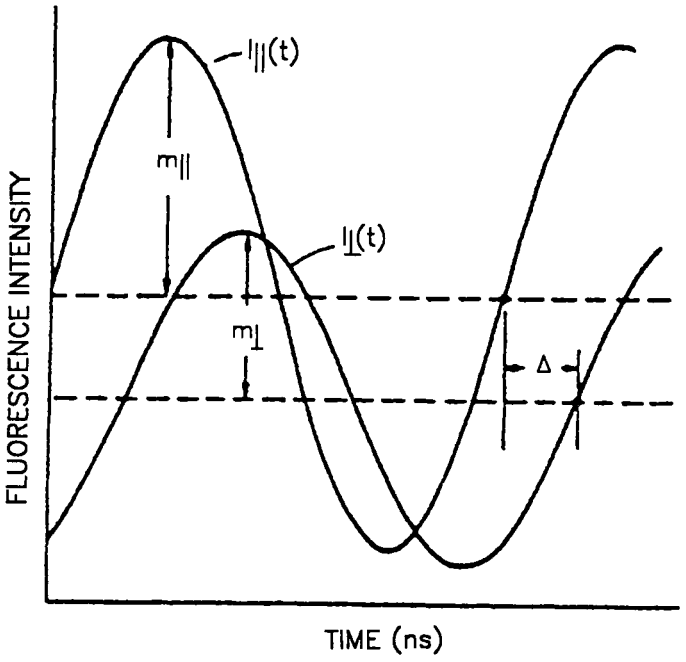

FIGURE 4. Schematic of the polarized modulation ratio (Λ; = $m_{\parallel}/m_{\perp}$) and the differential phase angle (Δ).

where r(t) is the time-resolved decay of the fluorescence anisotropy and I(t) is described by Equations 1 or 11. r(t) is a direct measure of the rotational dynamics of the systems. Its actual form depends on the assumed model, but the most common model predicts[25-27] that r(t) is described accurately by a multiexponential decay:

$$r(t) = r_o \sum_{i=1}^{n} g_i \exp(-t/\phi_i) \quad (20)$$

where r_o is the limiting anisotropy,[28] ϕ_i is the rotational correlation times, and g_i is the fractional contribution of each rotational correlation time to the total decay of anisotropy.

The majority of the rotational dynamics observed to date fall into four distinct categories: isotropic, anisotropic with two rotational correlation times, anisotropic with three rotational correlation times, and hindered rotation. Further detail on each model can be found in References 25 to 27. Regardless of the assumed r(t) model the calculated (c subscript) Δ_c and Λ_c are obtained from the polarized components of the sine and cosine Fourier transforms:[14]

$$S_i(\omega) = \int_0^\infty I_i(t) \sin \omega t \, dt \quad (21)$$

$$C_i(\omega) = \int_0^\infty I_i(t) \cos \omega t \, dt \quad (22)$$

where the subscript i is used to denote either $\parallel$ or $\perp$. From this it can be shown[14] that the resulting frequency-dependent values of Δ_c and Λ_c are given by

$$\Delta_c(\omega) = \arctan \{(C_\parallel S_\perp - C_\perp S_\parallel)/(S_\parallel S_\perp + C_\parallel C_\perp)\} \quad (23)$$

$$\Lambda_c(\omega) = (S_\parallel^2 + C_\parallel^2/S_\perp^2 + C_\perp^2). \quad (24)$$

The terms describing the decay of anisotropy (i.e., the rotational diffusion kinetics) are recovered by minimization of the χ^2 function:

$$\chi^2 = \frac{1}{D} \sum_\omega \left(\frac{\Delta_m(\omega) - \Delta_c(\omega)}{v_\Delta^2} \right)^2 + \frac{1}{D} \sum_\omega \left(\frac{\Lambda_m(\omega) - \Lambda_c(\omega)}{v_\Lambda^2} \right)^2 \quad (25)$$

where v_Δ and v_Λ represent the variances in the differential phase angle and polarized modulation ratio measurements, respectively. The remainder of the fitting protocol is identical to the description given previously for recovery of fluorescence lifetimes.

Figure 5 illustrates the experimental differential phase angle (panel A) and polarized modulation ratio data (panel B) for perylene in 1,2-propanediol. Clearly, a simple isotropic decay model (dotted line) does not accurately describe the experimental data. To successfully model the data, an anisotropic model with two rotational correlation times (solid line) is required. These results simply show that complex rotational dynamics can be recovered using frequency-domain fluorescence spectroscopy.

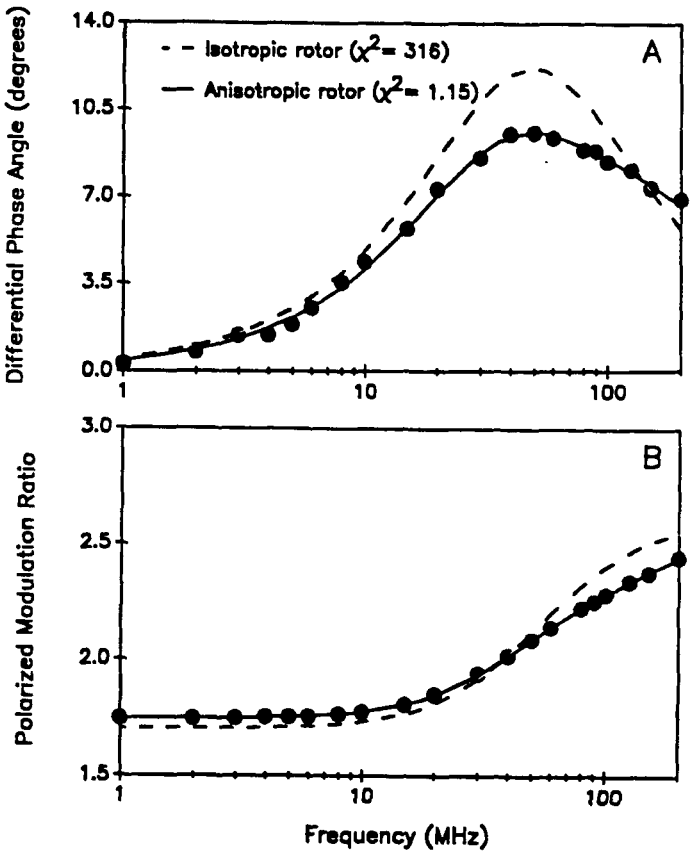

FIGURE 5. Multifrequency differential phase angle (A) and polarized modulation ratio (B) for perylene in 1,2-propanediol at 20°C. The curves are the best fits to isotropic (dotted line) and anisotropic rotor (solid line) models. The recovered rotational correlation times are 11.1 ns (87%) and 1.02 ns (13%).

III. INSTRUMENTATION

During the last decade, significant advances in instrumentation for time- and frequency-domain fluorescence spectroscopy have occurred. With present time-domain instrumentation and optical up-shifting techniques, femtosecond processes are now being explored.[29-31] In the frequency-domain, picosecond kinetics are routinely recovered and femtosecond experiments are on the immediate horizon. These advances have been made possible by the use of (1) excitation sources with large bandwidths and (2) detectors with high gain and wide bandwidths.

Table 2 compiles a listing of the milestones in frequency-domain fluorescence. This table traces the key instrumental advances from the earliest single frequency instrument of Gaviola[32] to the gigahertz multifrequency instrument in Lakowicz's laboratory.[33] Space precludes our discussing all the advances since 1926. For this reason we focus on the major advances that have occurred in the last 15 or so years leading up to the development of true multifrequency phase and modulation fluorometers.

Table 2
Key Instrumental Advances in Frequency-Domain Fluorometry

Year	Researcher(s)	Device
1926	Gaviola	Development of the first phase fluorometer
1953	Bailey/Rollefson	Electronic detection of the phase difference
1953	Birks/Little	Phase and modulation used
1969	Spencer/Weber	Electronic cross-correlation frequency down-shifting introduced
1975	Haar/Hauser	Continuously variable phase and modulation introduced
1977	Hieftje/Haugen/Ramsey	Intrinsic cavity mode noise used in frequency-domain fluorometry; only modulation information used
1979	Lytle/Pelletier/Harris	Pulsed laser excitation used in frequency-domain fluorometry; only phase angle information used
1980	Gratton/Lopez-Delgado	Harmonic content of a pulsed source and cross-correlation first proposed
1983	Gratton/Limkeman	First continuously variable phase and modulation fluorometer with cross-correlation detection
1984	Gratton/Jameson/ Rosato/Weber	First demonstration of the use of the harmonic content of a pulsed source for frequency-domain phase and modulation measurements
1985	Alcala/Gratton/Jameson	Harmonic content of a mode-locked laser used as an excitation source for phase and modulation fluorescence and cross-correlation detection
1986	Lakowicz and co-workers	Extension of harmonic approach to 2 GHz
1987	Hieftje and co-workers	Frequency-domain lifetime determinations via fiber optic light guides; only modulation information used
1988	Bright and co-workers	Fiber optic-based determination using phase-modulation and cross-correlation detection; rotational diffusion with fiber optic probes
1989	Gratton and co-workers	Parallel acquisition of phase and modulation information

A. Light Sources and Modulation Systems

The earliest instruments used Kerr cells as modulators and visual detection of the phase shift, but they suffered from poor UV transmission because the nitrobenzene used in the Kerr cell absorbed UV radiation. In addition, these early machines operated at relatively low frequencies. The Debye-Sears acousto-optic light modulator[34] allowed one to excite in the UV, but the system was usually limited to about three frequencies. A Debye-Sears-based system is still commercially available,[35] but has been superseded by true multifrequency instruments. Throughout the last decade, researchers realized the initial limitations in frequency-domain fluorescence was a lack of broadband multifrequency excitation sources.

The earliest attempts to develop true multifrequency instruments were undertaken by Haar and Hauser.[36] In their design, the cw output from a laser was modulated with an extracavity Pockel's cell. The frequency range of their most advanced instrument was reported to be 10 to 500 MHz. Very interesting rotational diffusion of rhodamine 6G in micelle solutions have been studied with this instrument.[37]

In 1977, Hieftje and co-workers[38] described an instrument that used the harmonic content of either a cw or pulsed laser as the excitation source for frequency-domain fluorescence. The sinusoidally modulated excitation frequencies (f) were obtained by using the intrinsic laser cavity resonant frequencies given by

$$f = nc/2L \tag{26}$$

where n is an integer, L is the laser cavity length, and c is the speed of light. Fluorescence decay times were recovered using only modulation information and a microwave spectrum analyzer was employed as the frequency-selective detector.

Lytle and co-workers[39] described a phase fluorometer that used optical heterodyning techniques to cover continuously the frequency range from 0.01 Hz to 1.2 GHz. In their design, a cavity dumper was used and the heterodyned optical beams were up- and down-shifted to cover the frequency range. Only phase angles were recorded and nothing more complex than single exponential decay times were explored.

One of the key problems encountered to this point was the inability to amplify easily the high frequency (mega- to gigahertz) photocurrents from the photomultiplier tube detector. Gratton and Lopez-Delgado[40] first discussed the possibility of using the harmonic content of a pulsed source for phase and modulation measurements with cross-correlation detection. Using cross-correlation detection one can electronically frequency down-shift the high-frequency fluorescence modulation to a

more manageable region (hertz), maintaining the phase and modulation information.[41] Thus, a superior instrument would result from using the high harmonic content of a pulsed source coupled to cross-correlation detection. However, it was not until 1984 that the first results appeared that fully demonstrated the possibilities of this approach.[16] The pulsed light source used for the particular experiments was the ADONE synchrotron storage ring in Frascati, Italy. Thus, the principle was demonstrated, but the practicality of performing experiments with a synchrotron source was quite problematic.

In 1983, Gratton and Limkeman[42] addressed the problems involved with using a synchrotron as a "routine" excitation source by developing the first continuously variable multifrequency phase and modulation fluorometer with cross-correlation detection. Figure 6 shows a block diagram of the instrument. Like the earlier instrument reported by Haar and coworkers,[36,37] the Gratton-Limkeman instrument used an extracavity Pockel's cell as the light modulator. A cw laser served as the light source and cross-correlation detection similar to that used in the synchrotron experiments was employed. The instrument operated continuously from 1 to 160 MHz and was used to recover accurately the individual decay times in multicomponent mixtures.

Alcala et al.[43] first introduced a cross-correlation multifrequency phase and modulation fluorometer that used the harmonic content of a mode-locked laser (Figure 7). In this instrument, the concepts first demonstrated by the Hieftje[38] and Lytle[39] groups were used with the improved electronic detection offered by cross-correlation. The impetus here was to increase the upper frequency limit of the earlier instrument,[42] and demonstrate that a less expensive (compared to a synchrotron) source could be used in frequency-domain fluorescence.

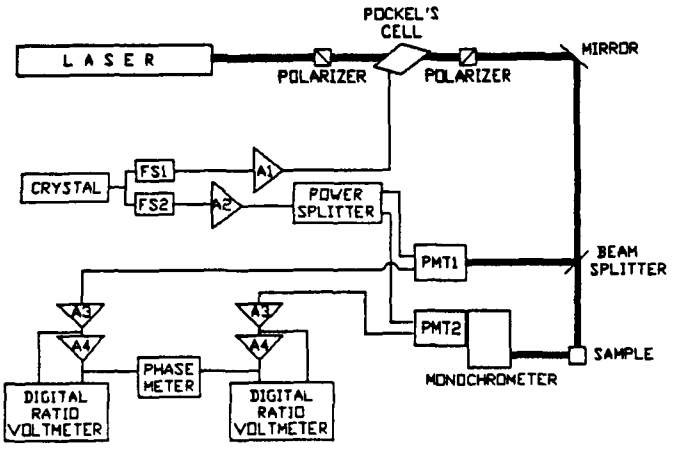

FIGURE 6. Schematic of the first continuously variable multifrequency phase and modulation fluorometer with cross-correlation detection. The bold lines denote optical paths. Abbreviations represent power amplifiers (A1, A2); amplifiers/filters (A3, A4); frequency synthesizers (FS1, FS2); and photomultiplier tube detectors (PMT1, PMT2).

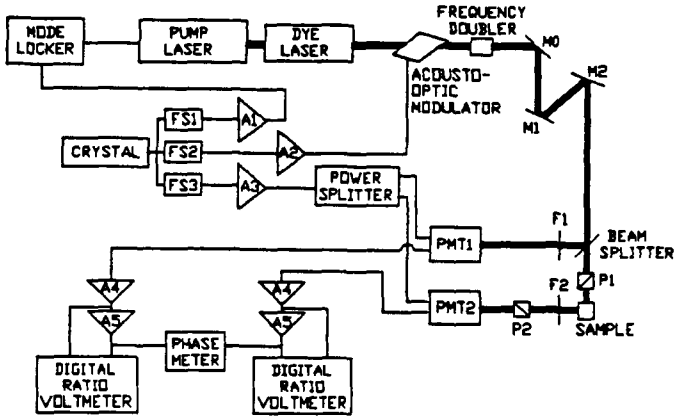

FIGURE 7. Schematic of the first continuously variable multifrequency cross-correlation phase and modulation fluorometer using the harmonic content of a mode-locked laser pulse train as the modulated light source. The bold lines denote optical paths. Abbreviations represent mirrors (M0, M1, M2); optical filters (F1, F2); photomultiplier tube detectors (PMT1, PMT2); optical polarizers (P1, P2); power amplifiers (A1, A2, A3); frequency synthesizers (FS1, FS2, FS3); and amplifiers/filters (A4, A5).

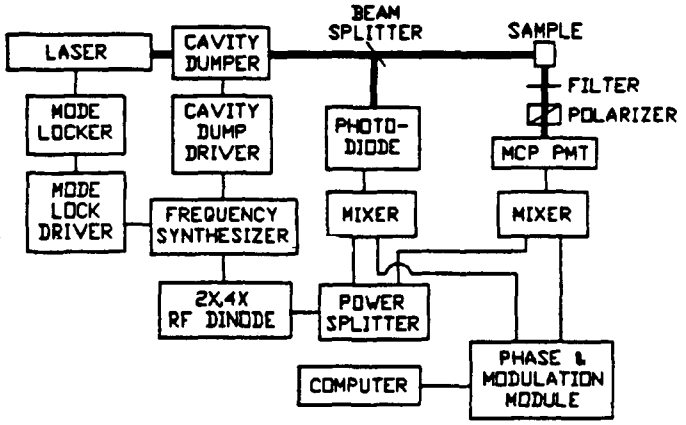

FIGURE 8. Schematic of the 2 GHz frequency-domain fluorometer constructed by Lakowicz and co-workers. The bold lines denote optical paths.

In operation, the output from a mode-locked laser is passed through an extracavity acousto-optic light modulator, generating side bands (sum and difference frequencies) onto the intrinsic harmonics that make up the mode-locked pulse train. By using this configuration, the upper frequency limit was extended to about 400 MHz. At this point, the photomultiplier tube detector became limiting.

In 1986, Lakowicz and co-workers[33] reported a phase-modulation fluorometer that operated to 2 GHz and used cross-correlation detection. Figure 8 shows a simplified schematic of this instrument which uses a cavity-dumped dye laser as the excitation source. With such a system one has an excitation source that is intrinsically modulated from about 4 MHz (i.e., the repetition rate of the cavity dumper), at 4 MHz intervals,

up to the bandwidth limit of the lasing medium (80 to 100 GHz for a dye laser).

A typical photomultiplier tube (PMT) with a rise time of 2 ns can only respond out to about 500 MHz. To circumvent this problem, Lakowicz and co-workers used a microchannel plate photomultiplier tube (MCP-PMT) as their detector. These devices have high gain and response times near 300 ps, and thus should operate up to several GHz.[33] Unfortunately, MCP-PMTs do not have discrete dynode chains, making internal cross-correlation[41] impossible. To circumvent this problem, Lakowicz and co-workers[33] developed a very clever postdetector cross-correlation mixing circuit. Using these two advances, Lakowicz's group extended the frequency range to 2 GHz.

One of the problems associated with all modern optical instrumentation is that they are not generally portable. Specifically, laser tables, lasers, sophisticated optics, and water and power requirements precludes the easy relocation of such equipment. To eliminate this problem for frequency-domain fluorescence instrumentation, Hieftje and co-workers[44] demonstrated the use of optical fibers as a means of transporting the excitation and fluorescence to and from remote locations. In this way, there is the possibility of performing nanosecond and sub-nanosecond kinetic measurements in hostile, remote, or inaccessible (*in vivo*) locations. Like the earlier instrumentation from the Hieftje group,[38] this fiber optic-based instrument only acquired modulation information, but the entire frequency spectrum could be acquired in only 15 ms.[44]

Our own group introduced the use of fiber optic sensors in concert with multifrequency phase and modulation fluorescence and cross-correlation detection.[45,46] The motivation for this design has been twofold. First, we hoped to increase the selectivity of fiber optic-based sensors by introducing time resolution. Second, we required instrumentation that would allow us to easily study the chemistry, biochemistry, and biophysics of molecules sorbed to surfaces. Figure 9 shows a block diagram of the instrument constructed in our laboratory. The excitation source is one of several cw lasers that is modulated by a Pockel's cell. The modulated radiation is then launched into either a single fiber arrangement[47] or a bifurcated fiber, as shown in Figure 9. Fiber lengths up to 175 m have been used and triple exponential decay times can be accurately recovered on sub-micromolar samples. In addition, phase resolved[48] and rotational diffusion[49] measurements have been performed with the same instrumentation.

The most recent advance in multifrequency phase and modulation fluorescence has been the development of instrumentation for the parallel acquisition of phase and modulation data.[50] In this design (Figure 10), the phase and modulation across the entire frequency spectrum (30 to 40 frequencies) can be collected simultaneously. Thus, experiments that took about 1 h can now be completed in <10 s.

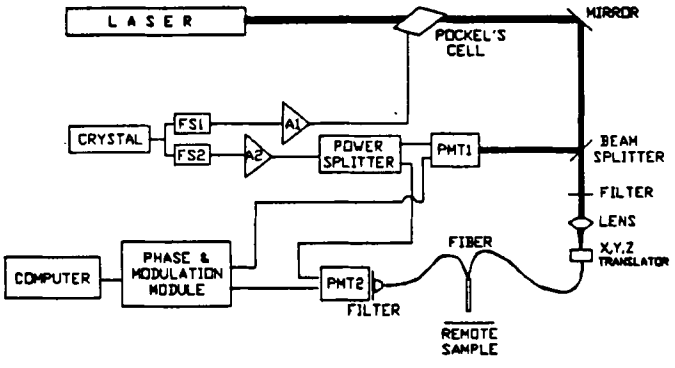

FIGURE 9. Schematic of the fiber optic-based multifrequency cross-correlation phase and modulation fluorometer constructed in the author's laboratory. The bold lines denote optical paths. Abbreviations represent power amplifiers (A1, A2); frequency synthesizers (FS1, FS2); and photomultiplier tube detectors (PMT1, PMT2).

B. Detectors

Presently, those of us practicing frequency-domain fluorescence spectroscopy are often driven to explore still faster processes. To this end, we are compelled to somehow increase the excitation modulation frequency. This point is illustrated in Figure 11, where we show the theoretically recovered fluorescence lifetime corresponding to a 1.0° phase shift as a function of the modulation frequency (dashed line). Clearly, as one would predict, the lifetime associated with a 1.0° phase shift decreases with increasing modulation frequency. Thus, in concept, femtosecond processes could be resolved by using (>10 GHz) modulation frequencies. However, all this assumes: (1) that the limiting noise sources are simply associated with the uncertainty in the phase measurements and (2) that a suitable ultrahigh bandwidth detector with suitable gain is available.

Unfortunately, both these assumptions are not met. For example, cw mode-locked, synchronously pumped, and cavity dumped laser systems now can provide modulation frequencies

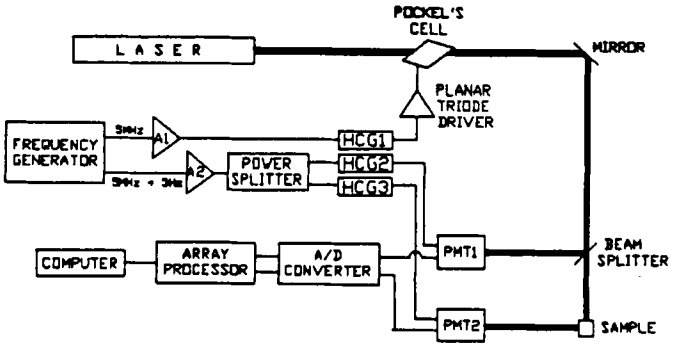

FIGURE 10. Schematic of the parallel acquisition multifrequency phase and modulation fluorometer. The bold lines denote optical paths. Abbreviations represent power amplifiers (A1, A2); photomultiplier tube detectors (PMT1, PMT2); and harmonic comb generators (HCG1, HCG2, HCG3).

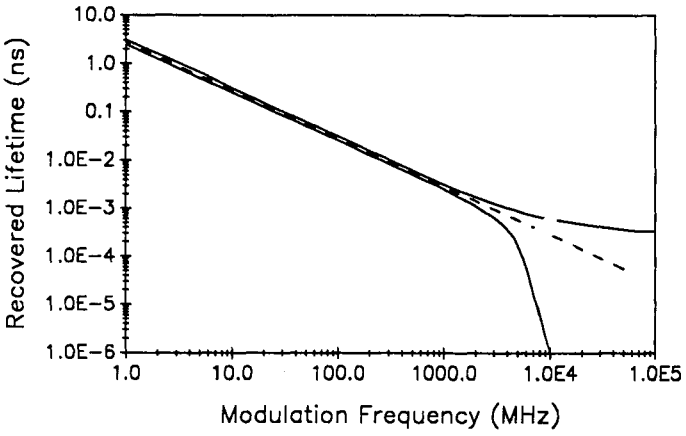

FIGURE 11. Recovered lifetime associated with a 1.0° phase shift vs. modulation frequency (dashed line). The region spanned by the two solid curves denotes the achievable precision assuming 300-fs pulse-pulse jitter.

to nearly 100 GHz, but they have a fundamental jitter of (under the best conditions) about 300 fs. Therefore, at higher modulation frequencies one becomes limited, not by the available modulation frequencies, but by the actual pulse-pulse time jitter. This effect is best shown by looking at the measurement precision or range (region spanned by the solid curves in Figure 11) of lifetime values that would be recovered at high modulation frequencies. Specifically, if we assume a 50 GHz modulation frequency and a hypothetical phase shift of 1.0° one would expect to recover a decay time of about 56 fs, but the precision of this measurement could not be any better than 300 fs (i.e., 56 ± 300 fs). To complicate issues further, no high gain detector exists that can respond above about 5 to 10 GHz and the vast majority operate below 1 GHz. Most common PMT detectors operate to about 500 MHz and MCP-PMTs can extend this range to at least 2 GHz.[33] Thus, the real keys to improving the time resolution of present day multifrequency fluorometers are twofold: (1) decrease the pulse-pulse jitter in the laser sources and simultaneously (2) increase the bandwidth of the detectors and maintain adequate gain.

IV. APPLICATIONS

A. Lifetimes

Much of the early multifrequency phase-modulation fluorescence work centered on the recovery of decay kinetics from synthetic multicomponent (multiexponential) samples.[10,11] The literature is ripe with examples of the power of the technique, and the interested reader should consult the earlier reviews in this field[10,11] and two joint papers by the Gratton and Lakowicz groups.[51,52]

There are two common techniques for measuring time-resolved fluorescence decays. The first is time-correlated single photon counting[2,8,9] and the second is phase and modulation fluorometry.[10,11] The two techniques are related to one another through the Fourier transform; however, it was not until recently that phase-modulation and time-correlated single photon counting were compared in an unbiased fashion. Prendergast and co-workers[53] were the first to construct a hybrid time- and frequency-domain instrument (Figure 12). Their results showed that the two methods recovered consistent decay times from samples that exhibit single or multi-exponential fluorescence decays. For example, the decay times for POPOP (*p*-bis[2-(5-phenyloxazolyl)]benzene) recovered using photon counting and phase-modulation were 1.315 ± 0.013 and 1.304 ± 0.003 ns, respectively. For more complex systems, these authors studied tryptophan emission from scorpion neurotoxin variant 3 (SN3) and ribonuclease T1 (RT1). The SN3 was best described by a triple exponential decay model, and the agreement between the sets of recovered parameters was reasonable. In contrast, RT1 (pH 5.5) was best described by a single exponential decay, and the agreement was excellent. Figures 13 and 14 illustrate the actual time- and frequency-domain data, respectively, for SN3 (panels a) and RT1 (panels b).

A stellar example of the time-resolving power of frequency-domain fluorescence has been reported by Lakowicz and coworkers.[54] These authors studied the sub-nanosecond kinetics of tyrosine emission from peptides and proteins. Figure 15

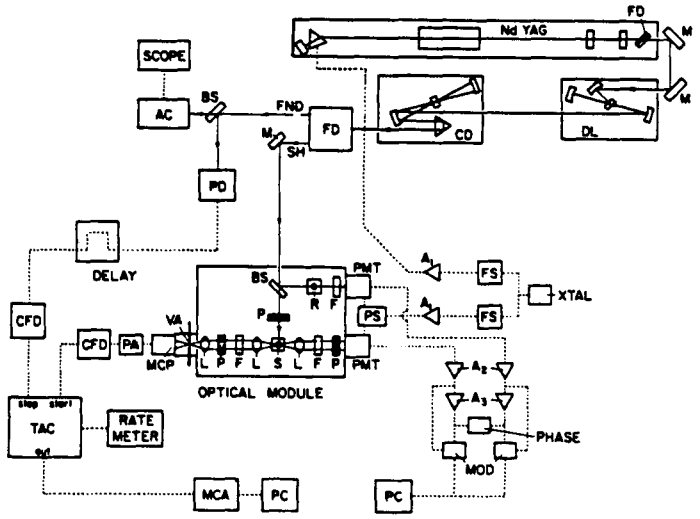

FIGURE 12. Schematic of the hybrid time-correlated single photon counting/multifrequency phase-modulation fluorometer constructed by Prendergast and co-workers. Abbreviation represent lens (L); optical filter (F); variable aperture (VA); photomultiplier tube (PMT); microchannel plate (MCP); power splitter (PS); RF amplifier (A1); DC amplifier (A2); AC tuned amplifier (A3); frequency synthesizer (FS); 10-MHz quartz oscillator (XTAL); preamplifier (PA); constant fraction discriminator (CFD); frequency doubler (FD); mirror (M); synchronously pumped dye laser (DL); cavity dumper (CD); dye laser fundamental (FND); dye laser second harmonic (SH); beam splitter (BS); real-time autocorrelator (AC); photodiode (PD); optical polarizer (P); sample (S). Solid lines trace out optic paths and dotted lines denote electrical connections. (From Hedstrom, J. et al., *Biochemistry*, 27, 6203, 1988. With permission.)

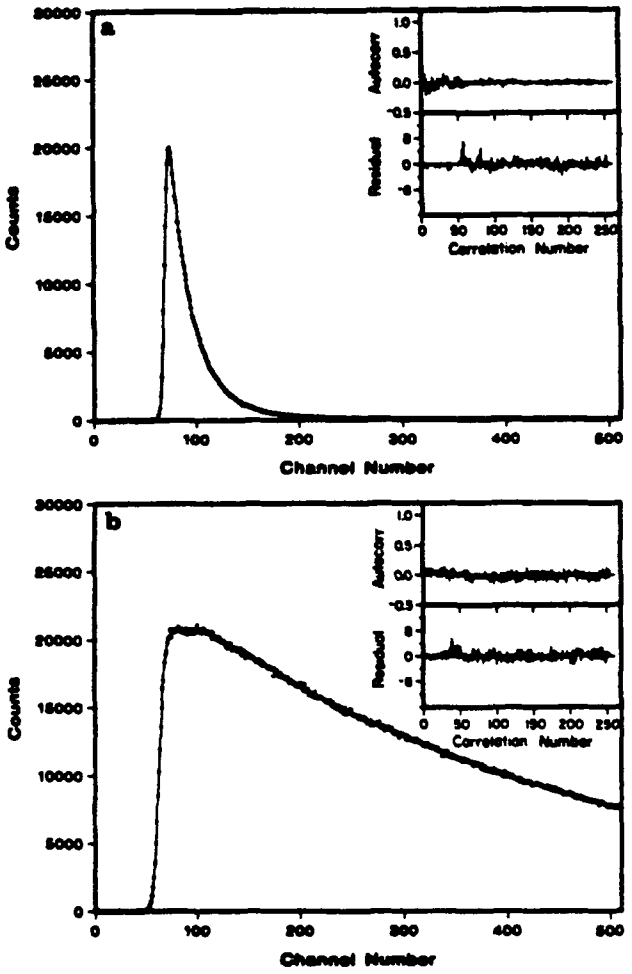

FIGURE 13. Time-domain fluorescence profiles of (a) SN3 in MOPS buffer (pH 7.0) and (b) RT1 in sodium acetate buffer (pH 5.5). Continuous curves are the optimized convolutions of triple (a) and double (b) exponential decay functions. The data are collected at 20-ps/channel in (a) and 10-ps/channel in (b). Lower and upper insets within each panel illustrate the residuals and autocorrelations of the residuals. (From Hedstrom, J. et al., *Biochemistry*, 27, 6203, 1988. With permission.)

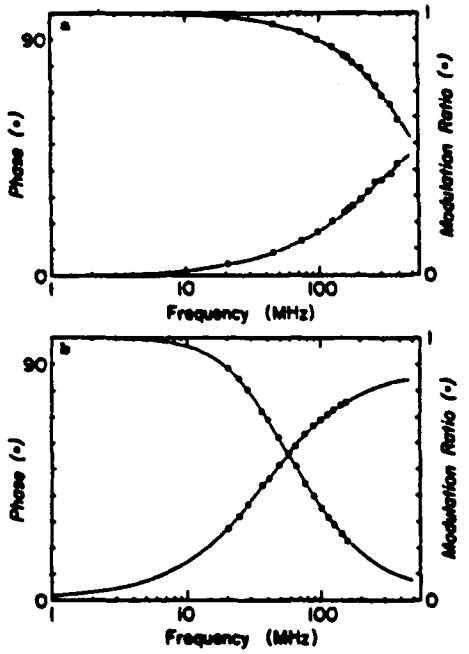

FIGURE 14. Multifrequency phase and modulation traces for the same SN3 (a) and RT1 (b) samples illustrated in Figure 13. The points represent the experimental data and the solid curves are the best fits to triple (a) and double (b) exponential decay functions. (From Hedstrom, J. et al., *Biochemistry*, 27, 6203, 1988. With permission.)

shows experimental data for oxytocin (upper panel) and bovine pancreatic trypsin inhibitor (BPTI; lower panel). For oxytocin, the data required at least three decay times for a good fit. Similarly, a double exponential function was needed to fit the BPTI data. In each case, all recovered decay times were less than 1 ns; however, no experiments were conducted to demonstrate the accuracy of the recovered parameters. Moreover, as has often been the case in protein studies, there is no clear physical meaning given to the two or three decay times from a protein system. This issue is addressed later in a discussion of results from lifetime distribution analyses.

Because of their unique organizational powers,[55] normal and reversed micelles have been an area of intense investigation. One way of studying the dynamics of micelles is to use a fluorescent probe. Elegant examples of such studies were reported by Valeur and co-workers.[56-58] These authors were concerned with determining the efficiency of proton transfer within the water pool of sodium bis(2-ethylhexyl) sulfosuccinate (AOT) reverse micelles using various polar fluorescent probes. In their initial studies,[56] the probe pyranine (Figure 16) was used. These authors found that the rate of reprotonation decreases and the rate of deprotonation increases as the water content w = $[H_2O]/[AOT]$ increases. However, at w = 12 the rates are comparable to that found in bulk water (Figure 17). These results were interpreted in terms of the proton hydration and salt effects.

McGown and Millican[59] have presented a theoretical discussion on the use of frequency-domain fluorescence spectroscopy as a selective "lifetime filter". Specifically, these authors discuss how phase-resolved fluorescence spectroscopy[6,60] can be used as a long-, short-, or bandpass filter function. Thus, if one wishes to selectively monitor a short-lived component, one would use a shortpass lifetime filter scheme, for example. Interestingly, these authors show that conventional time-domain experiments are restricted to longpass lifetime filtering. Therefore, there are significant advantages realized with the frequency-domain approach.

In the last few years, there has been a trend away from discrete decay times and toward the use of fluorescence lifetime distributions. However, as with any new method, one must take care in its application. Lakowicz and co-workers[61] have

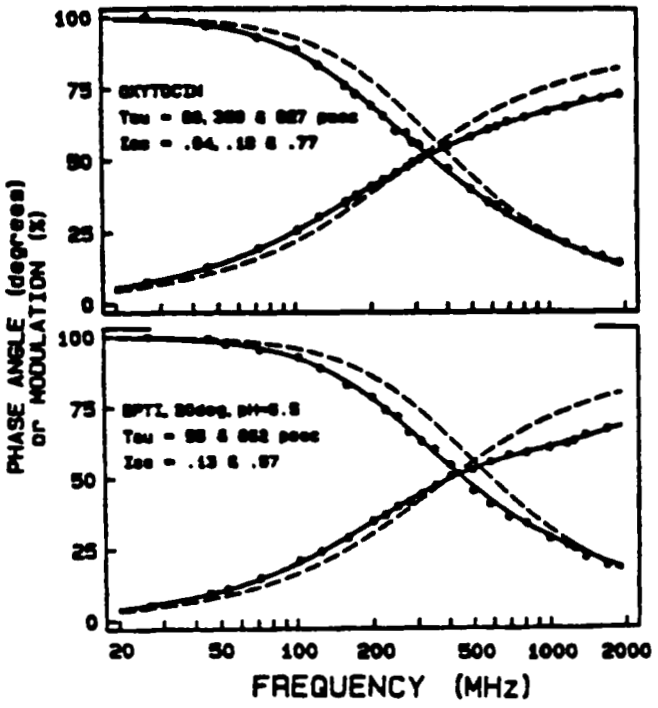

FIGURE 15. Multifrequency phase and modulation data (solid points) for oxytocin (upper) and BPTI (lower). The dashed curves represent the best single exponential fits to the data. The solid curves denote the best triple (upper) and double (lower) exponential fits to the data. The recovered decay times are indicated on the figure. (From Lakowicz, J. R. et al., *Biochemistry*, 26, 82, 1987. With permission.)

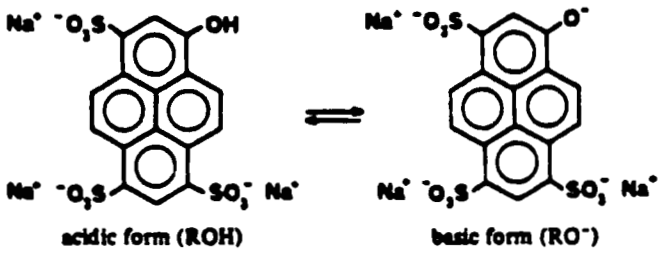

FIGURE 16. Acid and base forms of pyranine. (From Bardez, E. et al., *J. Phys. Chem.*, 88, 1909, 1984. With permission.)

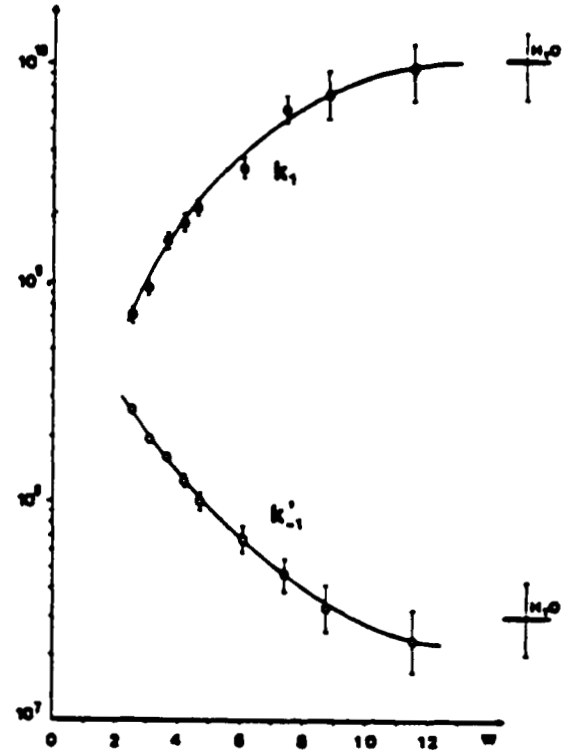

FIGURE 17. Variation in the recovered rate constants (y axis; s^{-1}) of deprotonation (k_1) and reprotonation (k'_1) vs. water content w. (From Bardez, E. et al., *J. Phys. Chem.*, 88, 1909, 1984. With permission.)

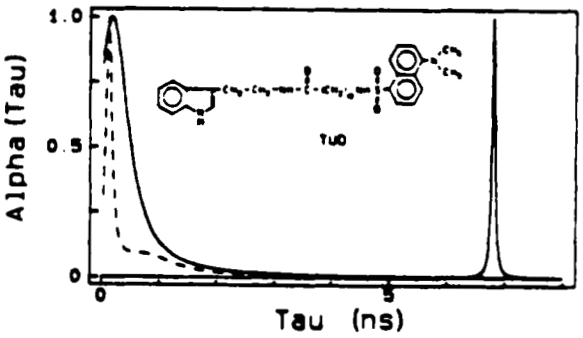

FIGURE 18. Lifetime distributions resulting from energy transfer with a range of donor-to-acceptor distances. Data are for tryptamine covalently attached to dansylundecanoic acid (TUD). The data are analyzed using uni- (solid line) and bimodal (dotted line) Lorentzian lifetime distributions. The solid trace centered at about 6.8 ns is in the absence of the acceptor, tryptamine-myristic acid. (From Lakowicz, J. R. et al., *Biophys. Chem.*, 28, 35, 1987. With permission.)

presented a detailed discussion of the practical aspects of analyzing complex decay kinetics using lifetime distribution analysis. These authors shows that it is always best to analyze complex data using a global analysis of multiple data sets. In this approach, multiple data sets are used and one searches solution space for a self-consistent set of kinetic parameters that simultaneously fit to all the data. In many cases, they report that ambiguous interpretation is possible if single experiments are analyzed alone. For example, a simulated unimodal lifetime distribution is often found to be well described by a discrete double exponential decay. The authors reported that a continuous lifetime distribution should be expected for time-dependent spectral relaxation of probe molecules associated with lipids, collisional quenching, distance-dependent energy transfer, and single tryptophan containing proteins. Figure 18 illustrates the recovered lifetime distribution resulting from energy transfer over a range of donor-to-acceptor dis-

tances. Similarly, Figure 19 shows results for the lifetime distributions of the single-tryptophan containing proteins monellin, melittin monomer, and RT1.

Eftink and Ghiron[62] also have studied RT1, globally fitting all their data simultaneously as a function of temperature and acrylamide quencher concentration. They concluded that they could not distinguish (based solely on the fitting statistics) a double exponential from a unimodal distribution fit. However, they argued quite convincingly that the observed preferential quenching of the short decay component of the discrete double exponential decay is strong evidence for a double exponential decay model.

Lifetime distribution analysis has also been applied to the study of solute decay kinetics in mixed solvent systems.[63] In these studies, Lakowicz and co-workers[63] showed that the decay kinetics for indole in cyclohexane/ethanol mixtures was best described by a bimodal distribution of decay times. Figure 20 shows typical lifetime distributions recovered for indole in various cyclohexane/ethanol mixtures.

Gratton and co-workers[64] have used lifetime distribution analysis to study the emission from sperm whale and tuna myoglobin. The authors found that the single-tryptophan-containing tuna myoglobin was described by a relatively narrow bimodal Lorentzian lifetime distribution. However, the two-tryptophan-containing sperm whale myoglobin was best described by a broad, unimodal lifetime distribution. Their conclusion was that the tuna myoglobin had a higher degree of structural flexibility compared to the sperm whale myoglobin.

Lakowicz and co-workers[65] have used lifetime distribution analysis coupled to resonance energy transfer to examine the distribution of distances between two sites on troponin I (TnI).

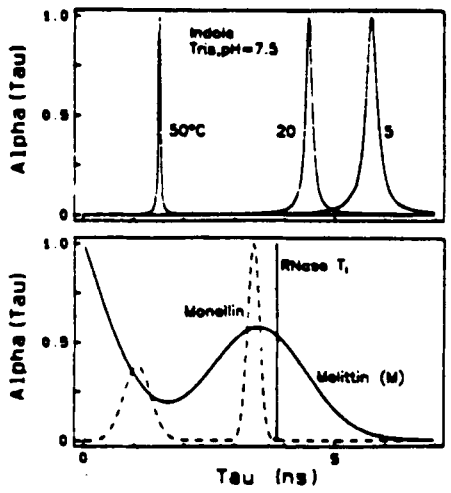

FIGURE 19. Lifetime distributions of single tryptophan proteins. (Upper) Distribution for the intensity decay of indole in water at various temperatures. (Lower) Decay-time distribution for monellin (dotted line), melittin monomer (solid line), and RT1. (From Lakowicz, J. R. et al., *Biophys. Chem.*, 28, 35, 1987. With permission).

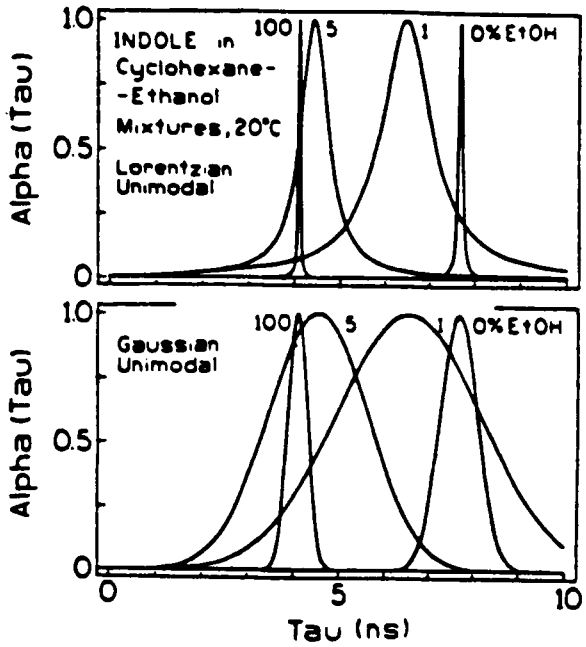

FIGURE 20. Distribution of lifetimes recovered for indole in cyclohexane/ethanol mixtures. (Upper) Unimodal Lorentzian. (Lower) Unimodal Gaussian. (From Gryczynski, I. et al., *Biophys. Chem.*, 32, 173, 1988. With permission.)

The donor was the single tryptophan residue at site 158 and the acceptor was cysteine 133 labeled with *N*-(iododacetyl)-*N'*-(1-sulfo-5-naphthyl) ethylene diamine. The recovered distance distribution between the donor and acceptor was betewen 2 and 3 nm.

Recently, our own group has investigated the decay kinetics of anilino naphthalene sulfonate (ANS) inclusion complexes with β-cyclodextrin.[66] In these studies, we used spectral, temporal, and thermodynamic information to argue that the observed decay kinetics for the inclusion complex is most accurately described by a unimodal lifetime distribution. Figure 21 shows a typical lifetime distribution recovered for 2,6-ANS complexed with β-cyclodextrin. The inclusion complexes on the figure illustrate proposed degrees of complexation. For example, when the complex is not completely formed, the decay time is short (quenched by water). When the complex is fully formed, the decay time is lengthened because the water cannot effectively quench the 2,6-ANS-β-cyclodextrin complex. At intermediate stages of complexation the lifetime distribution reflects the different extents of complex formation.

B. Rotational Dynamics

There is great interest in determining the rotational rates of species in solution. Much of the motivation for these studies, especially in protein systems, is the ability to compare one's results with molecular dynamics calculations.[67] The rotational dynamics of proteins can reveal the size, shape, and structural

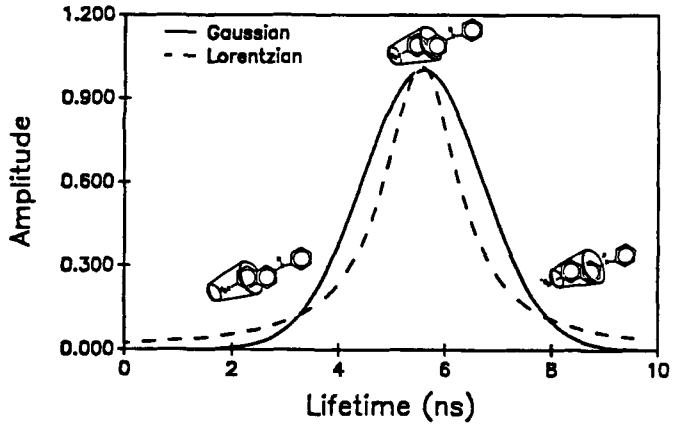

FIGURE 21. Recovered unimodal Gaussian (solid line) and Lorentzian (dotted line) lifetime distributions for 10^{-5} *M* 2,6-ANS in 10 m*M* β-cyclodextrin at 25°C. The inclusion complex structures represent possible conformations responsible for the lifetime distribution process. (From Bright, F. V. et al., *J. Am. Chem. Soc.*, 112, 1344, 1990.)

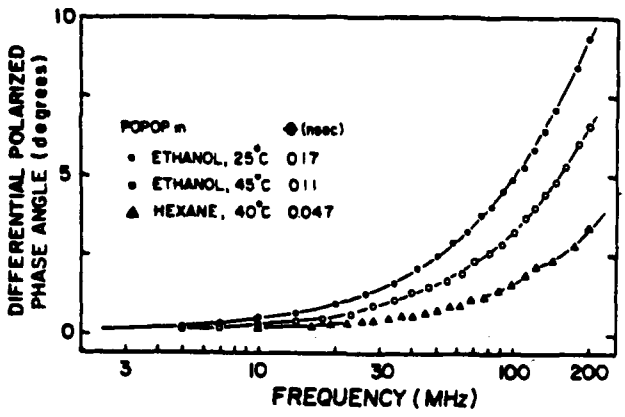

FIGURE 22. Differential polarized phase angle for POPOP in various solvents. (From Lakowicz, J. R. et al., *Anal. Instrum.*, 14, 193, 1985. With permission.)

rigidity. In other cases, rotational diffusion can give us insight into the (1) local environment surrounding a fluorescent probe, (2) extent of hydrogen bonding between the solute and the solvent; and (3) anisotropic rotational dynamics of many systems.

The use of frequency-domain fluorescence for the determination of rotational diffusion information was first described by Mantulin and Weber[24] and the associated theory presented by Weber.[14] In the earliest studies, these authors measured the differential phase angle (Equation 16) using one or two modulation frequencies and varied the rotational dynamics by adjusting the solvent viscosity. From these measurements, the authors proposed the concept of a tangent defect as a qualitative measure of the anisotropic nature of a rotor. A small tangent defect was indicative of a nearly isotropic rotor and a large defect corresponded to a strongly anisotropic rotor. These authors found that a probe that could hydrogen bond to the solvent inevitably behaved like an isotropic rotor. In contrast, a solute that did not hydrogen bond with the solvent (e.g., perylene in 1,2-propanediol) was described as an anisotropic rotor.

An example of the type of experimental data acquired using modern frequency-domain techniques is given in Figure 5. Similarly, Figure 22 shows the differential phase angle vs. modulation frequency traces for POPOP in ethanol and hexane.[68,69] The recovery of decay times below 50 ps (hexane, 40°C) is an indication of the time resolution possible with this technique. Inspecting these two examples (Figures 5 and 22) shows that anisotropic rotors and rapid rotational dynamics can be studied using frequency-domain fluorescence.

Chou and Wirth[70] have used multifrequency phase and modulation fluorescence to investigate the local environment around a fluorescent probe. The motivation for this work is to improve the understanding of small molecule solvation in bonded-phase liquid chromatography materials. To this end, these authors studied the rotational dynamics of acridine orange incorporated in sodium dodecyl sulfate (SDS) micelles. Because acridine orange is symmetric, the observed results could be interpreted quantitatively. The study showed that SDS-associated acridine orange rotates through an angle of only 45°. Complete rotation is hindered by the SDS association. Interestingly, results on premicellar aggregates indicated that these species "held" acridine orange more rigidly than an intact micelle.

One of the most difficult tasks in fluorescence spectroscopy is the recovery of accurate rotational diffusion kinetics from anisotropic systems. Lakowicz and co-workers[71] showed that by progressively quenching a sample they could selectively enhance the contribution of the shorter-lived rotational correlation time. For complex anisotropic decays, such as global and local motion of tryptophan residues within protein, these authors report significant increases in resolution by globally analyzing successively quenched samples. From these studies (Figures 23 and 24) the authors showed a substantial improvement in the resolution of 160 and 60 ps components in the monomeric and tetrameric forms of melittin, respectively.

Using the same global analysis scheme, Gryczynski et al.[72] were able to recover three rotational correlation times for the Y_t-base. In these experiments, both variable wavelength and quenching were used to recover rotational correlation times of 0.8, 3.0, and 5.6 ns. Typical multifrequency results are shown in Figure 25 and represent one of the few examples of a rigid rotor described clearly by three unique rotational correlation times.

In our group,[73] we used global analysis and multi-wavelength selectivity to develop fluorescence-anisotropy selective technique (FAST). Using this approach, we have shown how one can easily recover the emission spectra for the individual components in a binary mixture (Figure 26) when lifetime selectivity alone cannot effect a separation of the individual components.

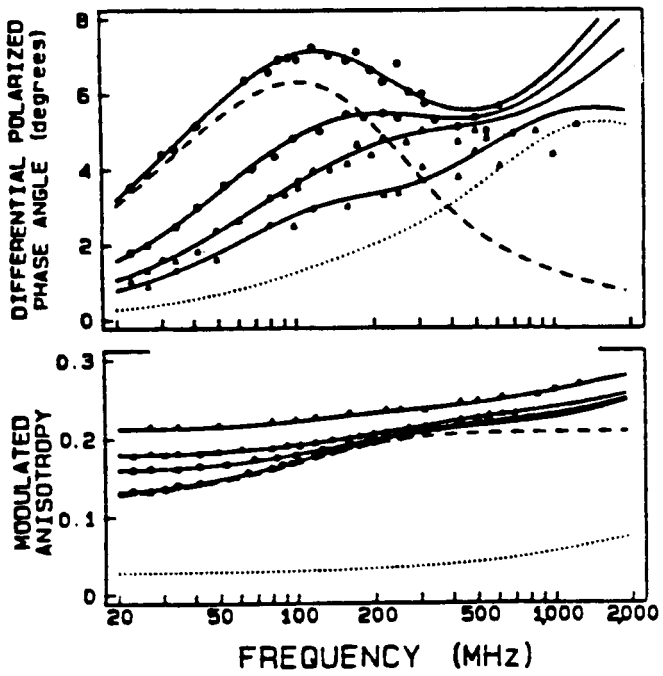

FIGURE 23. Frequency-domain anisotropy data for melittin tetrameter. Data are shown for acrylamide concentrations of 0, 0.2, 0.5, and 2.0 *M*. Solid curves are best global fits to anisotropic rotor models with two correlation times. The dotted and dashed curves are fits to inosotropic rotor models. (From Lakowicz, J. R. et al., *Biophys. J.*, 51, 755, 1987. With permission.)

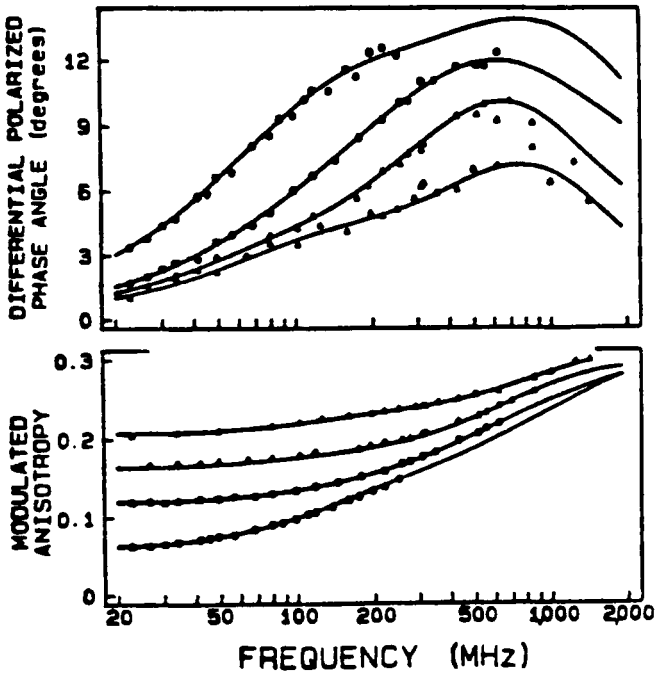

FIGURE 24. Frequency-domain anisotropy data for melittin monomer. Data are shown for acrylamide concentrations of 0, 0.2, 0.5, and 2.0 *M*. Solid curves are best global fits to anisotropic rotor models with two correlation times. (From Lakowicz, J. R. et al., *Biophys. J.*, 51, 755, 1987. With permission.)

V. PROSPECTUS FOR THE FUTURE

In the 7 years since the introduction of the first true multifrequency fluorometer,[42] there have been steady improvements in the initial design, but we are far from reaching the limits of the technique. Today's multifrequency fluorometers have been used extensively in the biochemical community for studying protein dynamics, etc., and only recently have practicing analytical chemists used the technique. The future of frequency-domain fluorescence is truly wide open and here we offer our ideas on areas where continued advances will be made.

First, there will be a steady increase in the time resolution of these instruments as faster, high gain detectors and more stable laser sources become available. The advances in microchannel plate photomultiplier tube technology will continue to improve and the practical limits of phase-modulation fluorescence should be approachable. In addition, it seems that the high gain avalanche photodiodes used by Berndt and coworkers[74,75] may also be applicable to GHz frequency-domain fluorescence.

Second, the data analysis algorithms will continue to proliferate. We have seen global analysis (for frequency-domain fluorescence) evolve during the last 5 years. In addition, the concepts of lifetime distribution analysis are finding widespread application in biochemistry and chemistry. Our own group has been using lifetime distribution analysis to study cyclodextrin and micelle systems and are now extending this approach to investigate the chemistry and biochemistry of species adsorbed or covalently attached at solid-liquid interfaces.

Third, with the advent of the true parallel fluorometers one will see more rapid (millisecond time scale) acquisition of experimental data. As a result, applications should appear in areas as diverse as the separation sciences and the kinetics of antigen-antibody formation at interfaces (e.g., a fiber optic sensor).[76]

Fourth, multidimensional data formats (Figure 27, for example) will continue to increase. Today, we find that three dimensions are used routinely, but the future will show that all possible fluorescence-based selectivity parameters (see Introduction) will be used in concert to increase selectivity.

Finally, by coupling parallel fluorescence[50] with fiber optic-based sensing we should soon be able to perform near real-time analysis on remotely located samples. Presently, much of the research is conducted at the laboratory site; however, with fiber optic probes we can begin to interrogate small, remote locations, with picosecond time resolution, in near real time.

ACKNOWLEDGMENTS

The work from our own laboratory was supported by BRSG SO7 RR 07066, awarded by the Biomedical Research Support

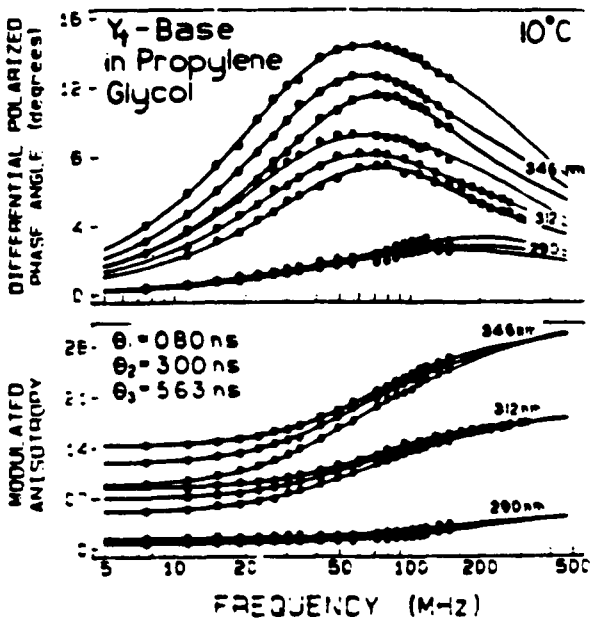

FIGURE 25. Frequency-domain differential phase and polarized modulation ratio data for Y_1-base in propylene glycol. In the upper panel, at each wavelength, the decreasing phase angles are for 0, 0.5, and 1.0 *M* CCl_4. In the lower panel, at each excitation wavelength, the increasing modulated anisotropy is for 0, 0.5, and 1.0 *M* CCl_4. (From Gryczynski, I. et al., *Biophys. Chem.*, 30, 271, 1988. With permission.)

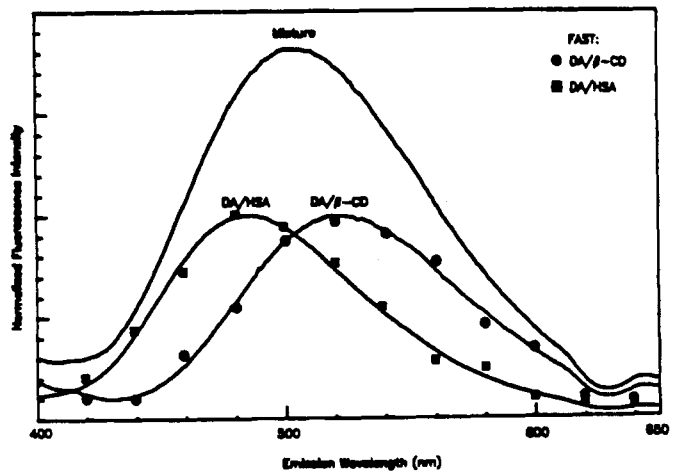

FIGURE 26. Steady-state emission spectra (solid curves) for dansylamide/β-cyclodextrin, dansylamide/human serum albumin, and 1:1 mixture. Points represent the FAST-resolved emission spectra for dansylamide/β-cyclodextrin and dansylamide/human serum albumin recovered from the 1:1 mixture. (From Bright, F. V., *Appl. Spectrosc.*, 42, 1245, 1988. With permission.)

Grant Program, Division of Resources, National Institutes of Health; the Donors of the Petroleum Research Fund, administered by the American Chemical Society (Grant #19620-G4); the Health Care Instruments and Devices Institute at SUNY-Buffalo; a Non-Tenured Faculty Grant from 3M, Inc.; a New Faculty Development Award from the New York State/United University Professions; the Center for Advanced Technology (SUNY-Buffalo); the Industry/University Cooperative Center for the Study of Biosurfaces (SUNY-Buffalo); the National Institute of Mental Health (Grant #MH43971); and the National Science Foundation (Grant #CHE-8921517). In addition, K. S. L. acknowledges support from an ACS Analytical Division Summer Fellowship sponsored by the Pittsburgh Conference. Finally, we thank Professors Eftink, Hieftje, Gratton, Jameson, Lakowicz, Prendergast, Wirth, McGown, Berndt, and Valeur for graciously providing us with reprints of their most recent work. Without their contributions this review would not have been possible.

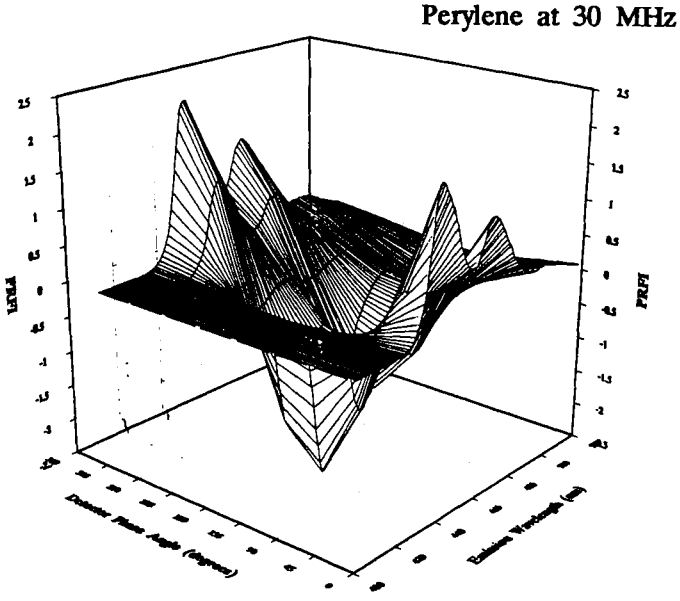

FIGURE 27. Illustration of a multidimensional data format of phase-resolved fluorescence intensity (PRFI), detector phase angle, and emission wavelength for 10^{-9} *M* perylene detected with a 175-m optical fiber probe.

REFERENCES

1. **Cundall, R. B. and Dale, R. E.,** *Time-Resolved Fluorescence Spectroscopy in Biochemistry and Biology,* Plenum Press, New York, 1980.
2. **Demas, J. N.,** *Excited State Lifetime Measurements,* Academic Press, New York, 1983.
3. **Lakowicz, J. R.,** *Principles of Fluorescence Spectroscopy,* Plenum Press, New York, 1983.
4. **Wehry, E. L., Ed.,** *Modern Fluorescence Spectroscopy,* Vol. 1 to 4, Plenum Press, New York, 1976.
5. **Warner, I. M., Patony, G., and Thomas, M. P.,** Multidimensional luminescence measurements, *Anal. Chem.*, 57, 463A, 1985.

6. **McGown, L. B. and Bright, F. V.,** Phase-resolved fluorescence in chemical analysis, *Crit. Rev. Anal. Chem.*, 18, 245, 1987.
7. **Bright, F. V.,** Bioanalytical applications of fluorescence spectroscopy, *Anal. Chem.*, 60, 1031A, 1988.
8. **Wirth, M. J.,** Picosecond spectroscopy in analytical chemistry, *Prog. Anal. Spectrosc.*, 11, 361, 1988.
9. **O'Conner, D. V. and Phillips, D.,** *Time Correlated Single Photon Counting*, Academic Press, New York, 1984.
10. **Gratton, E., Jameson, D. M., and Hall, R. D.,** Multifrequency phase and modulation fluorometry, *Annu. Rev. Biophys. Biophys. Bioeng.*, 13, 105, 1984.
11. **Jameson, D. M., Gratton, E., and Hall, R. D.,** The measurement and analysis of heterogeneous emissions by multifrequency phase and modulation fluorometry, *Appl. Spectrosc. Rev.*, 20, 55, 1984.
12. **Lakowicz, J. R., Lackzo, G., Gryczynski, I., Szmacinski, H., and Wiczk, W.,** Giga hertz frequency-domain fluorometry: resolution of complex decays, picosecond processes and future developments, *J. Photochem. Photobiol. B: Biol.*, 2, 295, 1988.
13. **Moore, J. H., Davis, C. C., and Coplan, M. A.,** *Building Scientific Apparatus: A Practical Guide to Design and Construction*, Addison-Wesley, Reading, MA, 1983, chap. 6.
14. **Weber, G.,** Theory of differential phase fluorometry: detection of anisotropic molecular motions, *J. Chem. Phys.*, 66, 4081, 1977.
15. **Bevington, P. R.,** *Data Reduction and Error Analysis for the Physical Sciences*, McGraw-Hill, New York, 1969.
16. **Gratton, E., Jameson, D. M., Rosato, N., and Weber, G.,** Multifrequency cross-correlation phase fluorometer using synchrotron radiation, *Rev. Sci. Instrum.*, 55, 486, 1984.
17. **Weber, G.,** Resolution of the fluorescence lifetimes in a heterogeneous system by phase and modulation measurements, *J. Phys. Chem.*, 85, 949, 1981.
18. **James, D. J. and Ware, W. R.,** A fallacy in the interpretation of fluorescence decay parameters, *Chem. Phys. Lett.*, 120, 455, 1985.
19. **James, D. J., Liu, Y.-S., DeMayo, P., and Ware, W. R.,** Distributions of fluorescence lifetimes: consequences of the photophysics of molecules adsorbed to surfaces, *Chem. Phys. Lett.*, 120, 460, 1985.
20. **James, D. R. and Ware, W. R.,** Recovery of underlying distributions of lifetimes from fluorescence decay data, *Chem. Phys. Lett.*, 126, 7, 1986.
21. **Alcala, J. R., Gratton, E., and Prendergast, F. G.,** Resolvability of fluorescence lifetime distributions using phase fluorometry, *Biophys. J.*, 51, 587, 1987.
22. **Alcala, J. R., Gratton, E., and Prendergast, F. G.,** Fluorescence lifetime distributions in proteins, *Biophys. J.*, 51, 597, 1987.
23. **Gryczynski, I., Wiczk, W., Johnson, M. L., and Lakowicz, J. R.,** Lifetime distributions and anisotropy decays of indole fluorescence in cyclohexane/ethanol mixtures by frequency-domain fluorometry, *Biophys. Chem.*, 32, 173, 1988.
24. **Mantulin, W. W. and Weber, G.,** Rotational anisotropy and solvent-fluorophore bonds: an investigation by differential polarized phase fluorometry, *J. Chem. Phys.*, 66, 4092, 1977.
25. **Chuang, T. J. and Eisenthal, K. B.,** Theory of fluorescence depolarization and anisotropic rotational diffusion, *J. Chem. Phys.*, 57, 5094, 1972.
26. **Cross, A. L. and Fleming, G. R.,** Analysis of time-resolved fluorescence anisotropy decays, *Biophys. J.*, 46, 45, 1984.
27. **Eisenthal, K. B.,** Studies of chemical and physical processes with picosecond lasers, *Acc. Chem. Res.*, 8, 118, 1975.
28. **Jablonski, A.,** On the notion of emission anisotropy, *Bull. Acad. Pol. Sci.*, 8, 259, 1960.
29. **Kahlow, M. A., Jarzeba, W., DuBruil, T. P., and Barbara, P. F.,** Ultrafast emission spectroscopy in the ultraviolet by time-gated upconversion, *Rev. Sci. Instrum.*, 59, 1098, 1988.
30. **Jarzeba, W., Wadler, G. C., Johnson, A. E., Kahlow, M. A., and Barbara, P. F.,** Femtosecond microscopic solvation dynamics of aqueous solutions, *J. Phys. Chem.*, 92, 7039, 1988.
31. **Kahlow, M. A., Jarzeba, W., Kang, T. J., and Barbara, P. F.,** Femtosecond resolved solvation dynamics in polar solvents, *J. Chem. Phys.*, 90, 151, 1989.
32. **Gaviola, Z.,** Ein Fluorometer. Apparat zur Messung von Fluoreszenzabklinggungszeinten, *Z. Phys.*, 42, 853, 1926.
33. **Lakowicz, J. R., Laczko, G., and Gryczynski, I.,** A 2 GHz frequency-domain fluorometer, *Rev. Sci. Instrum.*, 57, 2499, 1986.
34. **Debye, P. and Sears, F. W.,** On the scattering of light by supersonic waves, *Proc. Natl. Acad. Sci. U.S.A.*, 18, 409, 1932.
35. SLM-Aminco, Inc., Urbana, IL.
36. **Haar, H.-P. and Hauser, M.,** Phase fluorometer for measurement of picosecond processes, *Rev. Sci. Instrum.*, 49, 632, 1978.
37. **Klein, U. K. A. and Haar, H.-P.,** Picosecond time dependent rotational diffusion of rhodamine 6G in micellar solution, *Chem. Phys. Lett.*, 58, 531, 1978.
38. **Hieftje, G. M., Haugen, G. R., and Ramsey, J. M.,** New method for the determination of luminescence lifetimes by using the beat noise of a cw laser as a multifrequency-modulated source, *Appl. Phys. Lett.*, 30, 464, 1977.
39. **Lytle, F. E., Pelletier, M. J., and Harris, T. D.,** Intracavity laser intensity modulation at frequencies from 0.01 Hz to 1.2 GHz, *Appl. Spectrosc.*, 33, 28, 1979.
40. **Gratton, E. and Lopez-Delgado, R.,** Measuring fluorescence decay times by phase-shift and modulation techniques using the high harmonic content of pulsed light sources, *Nuovo Cimento*, 56B, 110, 1980.
41. **Spencer, R. D. and Weber, G.,** Measurements of subnanosecond fluorescence lifetimes with a cross-correlation phase fluorometer, *Ann. N.Y. Acad. Sci.*, 158, 361, 1969.
42. **Gratton, E. and Limkeman, M.,** A continuously variable frequency cross-correlation phase fluorometer with picosecond resolution, *Biophys. J.*, 44, 315, 1983.
43. **Alcala, J. R., Gratton, E., and Jameson, D. M.,** A multifrequency phase fluorometer using the harmonic content of a mode-locked laser, *Anal. Instrum.*, 14, 225, 1985.
44. **Bright, F. V., Monnig, C. A., and Hieftje, G. M.,** Rapid frequency-scanned fiber-optic fluorometer capable of subnanosecond lifetime determinations, *Anal. Chem.*, 58, 3139, 1986.
45. **Bright, F. V.,** Remote sensing with a multifrequency phase-modulation fluorometer, *SPIE Conf. Proc.*, 909, 23, 1988.
46. **Bright, F. V.,** A new fiber-optic-based multifrequency phase-modulation fluorometer, *Appl. Spectrosc.*, 42, 1531, 1988.
47. **Litwiler, K. S., and Bright, F. V.,** Multidimensional fluorescence with fiber-optic probes, in *Chemical Sensors and Microinstrumentation*, Vol. 403, Murray, R. W., Dessy, R. E., Heineman, W. R., Janata, J., and Seitz, W. R., Eds., 1989, chap. 25.
48. **Bright, F. V. and Litwiler, K. S.,** Multicomponent fluorimetric analysis using a fiber-optic probe, *Anal. Chem.*, 61, 1510, 1989.
49. **Betts, T. A., Bright, F. V., Catena, G. C., Huang, J., Litwiler, K. S., and Paterniti, D. P.,** Laser-based approaches to increase fiber-optic-based selectivity: dynamic fluorescence spectroscopy, in *Laser Techniques in Luminescence Spectroscopy*, Publ. No. 1066, Vo-Dinh, T. and Eastwood, D., Eds., American Society for Testing and Materials, Philadelphia, 1990, 88.
50. **Feddersen, B. A., Piston, D. W., and Gratton, E.,** Digital parallel acquisition in frequency domain fluorimetry, *Rev. Sci. Instrum.*, 60, 2929, 1989.
51. **Lakowicz, J. R., Laczko, G., Cherek, H., Gratton, E., and**

Limkeman, M., Analysis of fluorescence decay kinetics from variable-frequency phase shift and modulation data, *Biophys. J.*, 46, 463, 1984.

52. **Gratton, E., Limkeman, M., Lakowicz, J. R., Maliwal, B. P., Cherek, H., and Laczko, G.,** Resolution of mixtures of fluorophores using variable-frequency phase and modulation data, *Biophys. J.*, 46, 479, 1984.
53. **Hedstrom, J., Sedarous, S., and Prendergast, F. G.,** Measurements of fluorescence lifetimes by use of a hybrid time-correlated and multifrequency phase fluorometer, *Biochemistry*, 27, 6203, 1988.
54. **Lakowicz, J. R., Laczko, G., and Gryczynski, I.,** Picosecond resolution of tyrosine fluorescence and anisotropy decays by 2-GHz frequency-domain fluorometry, *Biochemistry*, 26, 82, 1987.
55. **Cline-Love, L. J., Habarta, J. G., and Dorsey, J. G.,** The micelle-analytical chemistry interface, *Anal. Chem.*, 56, 1133A, 1984.
56. **Bardez, E., Goguillon, B.-T., Keh, E., and Valeur, B.,** dynamics of excited-state reactions in reverse micelles. I. Proton transfer involving a hydrophilic fluorescent probe, *J. Phys. Chem.*, 88, 1909, 1984.
57. **Bardez, E., Monnier, E., and Valeur, B.,** Dynamics of excited-state reactions in reverse micelles. II. Proton transfer involving various probes according to their sites of solubilization, *J. Phys. Chem.*, 89, 5031, 1985.
58. **Bardez, E., Monnier, E., and Valeur, B.,** Absorption and fluorescence probing of the interface of aerosol OT reversed micelles and microemulsions, *J. Coll. Interface Sci.*, 112, 200, 1986.
59. **McGown, L. B. and Millican, D. W.,** Fluorescence lifetime selectivity in multifrequency phase-resolved fluorescence spectroscopy, *Appl. Spectrosc.*, 42, 1084, 1988.
60. **McGown, L. B. and Bright, F. V.,** Phase-resolved fluorescence spectroscopy, *Anal. Chem.*, 56, 1400A, 1984.
61. **Lakowicz, J. R., Cherek, H., Gryczynski, I., Joshi, N., and Johnson, M. L.,** Analysis of fluorescence decay kinetics in the frequency domain using distributions of decay times, *Biophys. Chem.*, 28, 35, 1987.
62. **Eftink, M. and Ghiron, C. A.,** Frequency domain measurements of the fluorescence lifetime of ribonuclease T_1, *Biophys. J.*, 52, 467, 1987.
63. **Gryczynski, I., Wiczk, W., Johnson, M. L., and Lakowicz, J. R.,** Lifetime distributions and anisotropy decays of indole fluorescence in cyclohexane/ethanol mixtures by frequency-domain fluorometry, *Biophys. Chem.*, 32, 173, 1988.
64. **Bismuto, E., Irace, G., and Gratton, E.,** Multiple conformational states in myoglobin revealed by frequency domain fluorometry, *Biochemistry*, 28, 1508, 1989.
65. **Lakowicz, J. R., Gryczynski, I., Cheung, H. C., Wang, C.-K., Johnson, M. L., and Joshi, N.,** Distance distribution in proteins recovered by using frequency-domain fluorometry. Applications to troponin I and its complex with troponin C, *Biochemistry*, 27, 9149, 1988.
66. **Bright, F. V., Catena, G. C., and Huang, J.,** Evidence for lifetime distributions in cyclodextrin inclusion complexes, *J. Am. Chem. Soc.*, 112, 1344, 1990.
67. **Ichiye, T. and Karplus M.,** Fluorescence depolarization of tryptophan residues in protein: a molecular dynamics study, *Biochemistry*, 22, 2884, 1983.
68. **Lakowicz, J. R., Gryczynski, I., and Wiczk, W. M.,** Anisotropic rotational diffusion of indole in cyclohexane studied by 2 GHz frequency-domain fluorometry, *Chem. Phys. Lett.*, 149, 134, 1988.
69. **Lakowicz, J. R., Maliwal, B. P., and Gratton, E.,** Recent developments in frequency-domain fluorometry, *Anal. Instrum.*, 14, 193, 1985.
70. **Chou, S.-H. and Wirth, M. J.,** Rotational diffusion of acridine orange attached to SDS micelles, *J. Phys. Chem.*, 93, 7694, 1989.
71. **Lakowicz, J. R., Cherek, H., Gryczynski, I., Joshi, N., and Johnson, M. L.,** Enhanced resolution of fluorescence anisotropy decays by simultaneous analysis of progressively quenched samples, *Biophys. J.*, 51, 755, 1987.
72. **Gryczynski, I., Cherek, H., and Lakowicz, J. R.,** Detection of three rotational correlation times for a rigid asymmetric molecule using frequency-domain fluorometry, *Biophys. Chem.*, 30, 271, 1988.
73. **Bright, F. V.,** Fluorescence anisotropy selective technique (FAST): a new approach to multicomponent fluorimetric analysis, *Appl. Spectrosc.*, 42, 1245, 1988.
74. **Berndt, K.,** Application of gain-modulated avalanche photodiodes in phase-sensitive fluorescence spectroscopy, *Opt. Commun.*, 56, 30, 1985.
75. **Berndt, K.,** Picosecond opto-electronic cross-correlator with single-photon sensitivity, *Opt. Commun.*, 61, 33, 1987.
76. **Bright, F. V., Betts, T. A., and Litwiler, K. S.,** Regenerable fiber-optic-based immunosensor, *Anal. Chem.*, 62, 1065, 1990.